Bis-nor-diterpene from Cnidoscolus quercifolius (Euphorbiaceae) induces tubulin depolymerization-mediated apoptosis in BRAFmutated melanoma cells

Raimundo Gonçalves de Oliveira-Júnior, Christiane Adrielly Alves Ferraz, Ana Paula de Oliveira, Edigênia Cavalcante da Cruz Araújo, Grégoire Prunier, Laureen Beaugeard, Hugo Groult, Laurent Picot, Edilson Beserra de Alencar Filho, Noureddine El Aouad, et al.

Bis-*nor*-diterpene from *Cnidoscolus quercifolius* (Euphorbiaceae) induces tubulin depolymerization-mediated apoptosis in BRAF-mutated melanoma cells

Raimundo Gonçalves de Oliveira-Júnior[a], Christiane Adrielly Alves Ferraz[a], Ana Paula de Oliveira[a], Edigênia Cavalcante da Cruz Araújo[a], Grégoire Prunier[b], Laureen Beaugeard[b], Hugo Groult[b], Laurent Picot[b], Edilson Beserra de Alencar Filho[c], Noureddine El Aouad[d], Larissa Araújo Rolim[a], Jackson Roberto Guedes da Silva Almeida[a,*]

[a]Center for Studies and Research of Medicinal Plants, Federal University of San Francisco Valley, 56304-205, Petrolina, Pernambuco, Brazil.

[b] LIENSs UMR CNRS 7266, La Rochelle Université, 17042 La Rochelle, France.

[c] Department of Pharmacy, Federal University of San Francisco Valley, 56304-205, Petrolina, Pernambuco, Brazil.

[d] Research Team on Biological Engineering, Agrifood and Aquaculture, Polydisciplinary Faculty of Larache, Abdelmalek Essaadi University, Tetouan, Route de Rabat, 92000, Larache, Morocco.

*Corresponding author: Federal University of San Francisco Valley. Av. José de Sá Maniçoba, S/N, Centro, 56304-205, Petrolina, Pernambuco, Brazil. E-mail address: jackson.guedes@univasf.edu.br (Jackson Roberto Guedes da Silva Almeida).

ABSTRACT

A phytochemical investigation of cytotoxic extract and fractions of *Cnidoscolus quercifolius* Pohl led to isolation of five terpenoids, including three lupane-type triterpenes (**1-3**) and two bis-*nor*-diterpenes (**4-5**). Compounds **4** (phyllacanthone) and **5** (favelanone) are commonly found in this species and have unique chemical structure. Although their cytotoxic activity against cancer cells has been previously reported, the anticancer potential of these molecules remains poorly explored. In this paper, the antimelanoma potential of phyllacanthone (PHY) was described for the first time. Cell viability assay showed a promising cytotoxic activity (IC_{50} = 40.9 µM) against chemoresistant human melanoma cells expressing the BRAF oncogenic mutation (A2058 cell line). After 72 h of treatment, PHY inhibited cell migration and induced apoptosis and cell cycle arrest ($p < 0.05$). Immunofluorescence assay showed that the pro-apoptotic effect of PHY is probably associated with tubulin depolymerization, resulting in cytoskeleton disruption of melanoma cells. Molecular docking investigation confirmed this hypothesis given that satisfactory interaction between PHY and tubulin was observed, particularly at the colchicine binding site. These results suggest PHY from *C. quercifolius* could be potential leader for the design of new antimelanoma drugs.

Keywords: apoptosis; cancer; cytoskeleton; diterpene; melanoma.

Highlights

- Bioguided purification led to the isolation of phyllacanthone (PHY) from *C. quercifolius.*
- PHY inhibited cell proliferation and migration, and induced apoptosis and cell cycle arrest.
- Pro-apoptotic effect of PHY was associated with tubulin depolymerization.
- New PHY-structure based molecules could be designed to obtain antimelanoma drug candidates.

1. Introduction

Melanoma is an aggressive malignant tumor derived from melanocytes. Although it represents only 2% of all skin cancer cases, melanoma is responsible for about 90% of total skin cancer-related deaths [1]. Its aggressive nature is mainly explained by genomic alterations and their post-transcriptional consequences [2]. Melanoma cells express proliferative signaling pathways that are constitutively activated. Overactivation of the RAS-RAF-MEK pathway is observed in about 90% of melanomas and the predominant mutation affects the BRAF gene in 50-70% of cases. Its tumor progression is strongly associated with apoptosis escape mechanisms, neovascularization stimulation, up-regulation of immunosuppressive factors and inhibition of immune checkpoints [3,4].

Antimelanoma therapy includes the use of cytokines (e.g. IL-2 and IFN-α), as well as monoclonal antibodies (e.g., CTLA-4 and PD-1/2 receptor inhibitors) that reactivate immune checkpoints, enhancing the lymphocyte antitumor response [5,6]. Another recent therapeutic approach is based on the use of cytotoxic molecules targeting mutated signaling pathways. BRAF inhibitors (e.g., vemurafenib, dabrafenib and encorafenib) and MEK inhibitors (e.g., cobimetinib, trametinib and binimetinib) are the main representatives of targeted therapy and offer a better anti-tumor response compared to conventional anticancer drugs such as alkylating agents, antimitotic agents, and other apoptosis inducers [7-9]. However, tumor response to targeted therapy is not sustained on a long-term basis due to resistance mechanisms acquired during treatment, which requires the use of increasing doses. In this sense, the search for new anti-melanoma molecules remains a challenge for researchers in the field.

Cnidoscolus quercifolius Pohl (syn. *C. phyllacanthus* (Mull. Arg.) Pax & L. Hoffm.) is a Brazilian medicinal plant, endemic to the Caatinga biome and popularly known as “favela”, “faveleira” or “urtiga-branca”. In folk medicine, this species is commonly used to treat

hemorrhoids, kidney disorders, ophthalmological diseases, injuries, urinary tract infection and inflammation [10]. Phytochemical studies have reported the isolation of lupane-type triterpenes and bis-*nor*-diterpenes from *C. quercifolius* (syn. *C. phyllacanthus*) [11-15]. Previous pharmacological investigations have evaluated the antiproliferative effect of ethanol extracts from *C. quercifolius* [16]. Bis-*nor*-diterpenes isolated from *C. quercifolius* showed significant cytotoxic effect on several tumor cell lines, including breast (MCF-7), leukemia (HL-60 and P-388), and lung (NCI-H292) cancer cells [17]. Nevertheless, the antimelanoma potential of *C. quercifolius* and its isolated compounds is still unknown. In this paper, we have described a bioguided purification that has led to the isolation of a bis-*nor*-diterpene (phyllacanthone, PHY) with cytotoxic activity against human melanoma cells expressing the oncogenic BRAF mutation.

2. Materials and Methods

2.1. Plant material

Stembarks of *C. quercifolius* were collected in a typical Caatinga area, located in Petrolina, state of Pernambuco, Brazil (Coordinates: 09° 03' 55.30'' S, 040° 20' 06.90'' W), in February 2013. Botanical identification was confirmed by Viseldo Ribeiro de Oliveira, and a voucher specimen (n° 19202) has been deposited at the *Herbário Vale do São Francisco* (HVASF), *Universidade Federal do Vale do São Francisco* (UNIVASF). All procedures for access to genetic patrimony and associated traditional knowledge were carried out and the project was registered in SisGen (Register #A65F584).

2.2. General

^{1}H and ^{13}C NMR spectra were obtained on a Bruker Ascend spectrometer operating at 400 and 100 MHz, respectively. NMR spectra were obtained in deuterated chloroform ($CDCl_3$) using tetramethylsilane (TMS) as an internal standard, with chemical shifts expressed in ppm (δ) and coupling constants (*J*) in Hz.

2.3. Extraction and bioguided fractionation

Dried and pulverized stembarks of *C. quercifolius* (1,481 g) were extracted with ethanol, yielding 392 g of ethanol extract (EE, 26.46%). During the preparation of EE, it was observed the formation of a white precipitate that, after repeated washing with methanol, resulted in 26 mg of white colored crystals (mixture of compounds **1** and **2**), soluble in chloroform. An aliquot of EE (50 g) was fractioned by column chromatography under vacuum (CCUV), using silica gel 60 (230-240 mesh, 500 g) as stationary phase. Hexane, chloroform, ethyl acetate and methanol were used as solvents, in increasing order of polarity, yielding hexane (0.13 g), $CHCl_3$ (16.59 g), AcOEt (10.26 g) and MeOH (21.44 g) fractions, respectively. After pharmacological evaluation, $CHCl_3$ fraction (12 g) was fractionated by CCUV (silica gel 60, 240 g), using hexane (3.0 l), hexane-$CHCl_3$ (1:1, 3.0 l), $CHCl_3$ (2.0 l), $CHCl_3$-AcOEt (1:1, 2.0 l), AcOEt (1.0 l) and MeOH (1.0 l) as solvents, resulting in six subfractions of different polarity. Hexane-$CHCl_3$ (1:1) subfraction (2.7 g) was loaded to preparative TLC and eluted with hexane-AcOEt (92.5:7.5, *v/v*), resulting in the isolation of compounds **3** (91 mg, white solid), **4** (402 mg, yellow crystals) and **5** (12 mg, colorless crystals), all soluble in $CHCl_3$ (Figure 1).

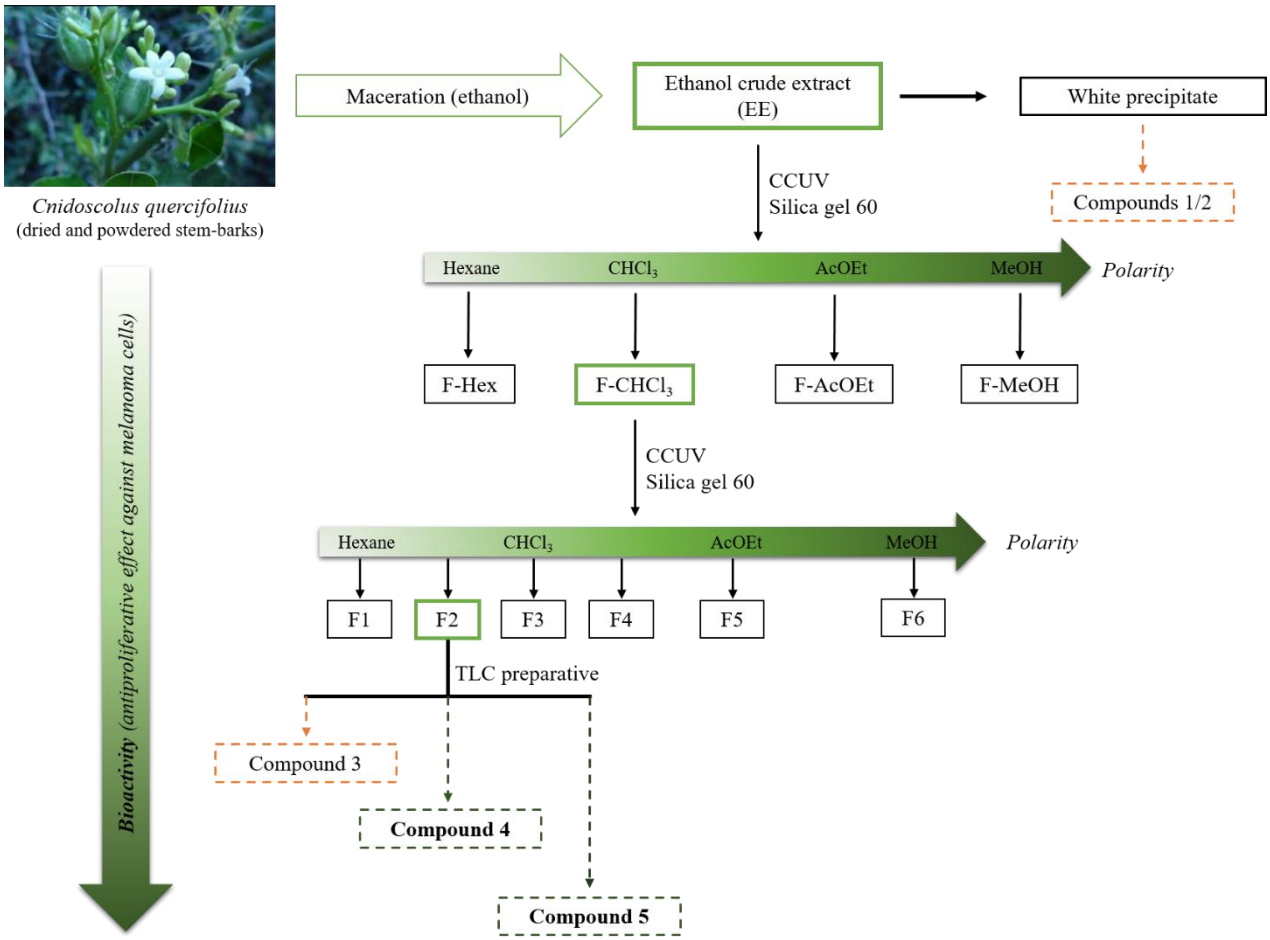

Figure 1. General bioguided fractionation scheme of *Cnidoscolus quercifolius* stembarks.

2.4. Cell culture

All pharmacological assays were performed using A2058 (ATCC® CRL-11147™) cell line. A2058 are highly invasive epithelial adherent melanoma cells expressing the $BRAF^{V600E}$ oncogenic mutation [18]. They are tumorigenic at 100% frequency in nude mice, and considered as resistant to conventional anticancer drugs [19]. Cells were grown to confluence in 75 cm² flasks in DMEM supplemented with 10% fetal calf serum (FCS) and 1% penicillin-streptomycin, in a 5% CO_2 (37 °C) humidified atmosphere.

2.5. Cell viability assay

Samples were solubilized in DMSO before dilution in the cell culture medium. The DMSO final concentration was lower than 1% and tested as negative control. A2058 cells (2 x 10^3/well) were treated with EE and fractions (25–400 µg/mL) and isolated compounds (1–200 µM). Vemurafenib (1–200 µM) was used as standard drug. After 72h, cell viability was measured using the MTT assay as previously described [20,21]. Cell morphology was evaluated after treatments under inverted phase contrast microscope (Nikon, Eclipse, France). IC_{50} was calculated by nonlinear regression analysis using Prism 6.0 (GraphPad Software).

2.6. Annexin-V/6-CFDA assay

Melanoma cells were incubated in 4-well slides (5 x 10^3/well) for 24 h and then exposed to PHY (20, 50 and 100 µM) during 72 h. After treatments, cells were washed with PBS and double stained with annexin V-Cy3 (red fluorescence) and 6-carboxyfluorescein diacetate (6-CFDA, green fluorescence) solution, according to manufacturer's recommendations (Sigma-Aldrich®, France). Cells were observed under fluorescence microscope (ZEISS Axion Observer, France) [19].

2.7. Caspase-3 activity

Caspase-3 activity was determined using a colorimetric assay (CASP3C kit, Sigma-Aldrich®, France) as previously reported. Cells (2.5 mL of a cell suspension at 5 x 10^5 cel.mL^{-1}) were incubated in 75 cm^2 flasks and exposed to cell culture medium (12.5 mL, negative control) or PHY (20, 50 and 100 µM) for 72 h. After treatments, cells were washed with PBS, lysed with lysis buffer and the caspase activity (µmol pNA/min/mL) was measured according to manufacturer's recommendations.

2.8. Cell cycle analysis

Cell cycle analysis was performed by flow cytometry, using propidium iodide (PI) staining. Melanoma cells were grown in control culture medium or treated with PHY (20, 50 and 100 µM) for 72 h. Then, cells were stained in PBS containing PI 100 $\mu g.mL^{-1}$, RNAse A 100 $\mu g.mL^{-1}$ and 0.1% Triton X-100 (ThermoFisher Scientific, France), at 37 °C for 15 min. After staining, melanoma cells were analyzed using a FACS Cantoll flux cytometer (BD Biosciences, France) equipped with an air cooled blue LASER (λ = 488 nm, 20 mW), as previously described [19,22].

2.9. Cell migration assay

Cell migration was determined by the wound healing assay as previously described [23]. A2058 cells (2 x 10^3/well) were grown in 24-well plates to 90% confluence. Cell monolayers were scratched with a sterile plastic tip, washed with PBS solution and incubated in a new cell culture medium containing PHY (20 and 50 µM) for 24 h. Cell migration was recorded using a ZEISS Axion Observer microscope in living cell mode (one photomicrograph every 10 min). Cell migration was calculated at 0, 3, 6, 12 and 24h of treatment by measuring the cell surface using ImageJ® software.

2.10. Immunofluorescence assay for α-tubulin staining

A2058 cells were grown in 4-well culture slides (1 x 10^4/well) for 24 h, washed with PBS and then exposed to PHY (20, 50 and 100 µM) or nocodazole (50 nM) for 24 h. Cells were fixed with 4% paraformaldehyde in PBS, for 15 min at 37 °C. After fixation, cells were permeabilized and saturated with a 3% BSA solution containing 0.1% Triton X100 in PBS, and then incubated overnight at 4 °C with a mouse anti-α-tubulin-FITC monoclonal antibody (Sigma-Aldrich®, France) at 1:50 dilution in PBS. Cells were washed with PBS and nucleus staining was performed with a DAPI solution during 15 min at room temperature.

Photomicrographs were taken on a Zeiss fluorescence microscope (ZEISS Axion Observer, France).

2.11. Docking study

Molecular docking was performed to investigate the possible interaction modes of PHY with tubulin. The analyses were made using as standard two different crystallographic complexes, containing nocodazole or colchicine, which are compounds slightly displaced in near binding sites between the A and B domains of tubulin [24]. These complexes were obtained from RCSB protein data bank [24,25] (https://www.rcsb.org/), under the codes PDB IDs: 4O2B and 5CA1. These two complexes were chosen because nocodazole was used in experimental protocols and colchicine has a remarkably similar structure with PHY, having both the same mechanism of action in near sites. In view of this, both complexes were considered as important molecular hypotheses for comparisons.

All the calculations were made using the Autodock Vina [26] module of Autodock and AutodockTools packages [27]. Vina contains a more recent algorithm that provides better results in comparison with the original Algorithms of Autodock, with a smallest computational coast [26].

Before docking procedures, an initial geometry optimization of the non-crystallographic ligand was made through the PM3 semiempirical Hamiltonian, using the Gaussian 09W package [28], at CENAPAD-UFC cluster architecture (http://www.cenapad.ufc.br/). Redocking procedure was performed using the crystallographic structure of colchicine and nocodazole complexes, considering a grid box with dimensions of 14 x 14 x 14 Å and internal spacing of 1.0 Å (default of Vina). The same parameters were used for the docking of PHY. 3D and 2D images were generated respectively with Chimera 1.13.1rc [29] and Biovia Discovery Studio Visualizer [30].

2.12. Statistical analysis

All results are presented as mean ± standard error of the mean (SEM), from at least three independent measurements (n=3). Statistical analysis was performed using one-way analysis of variance (ANOVA) followed by Dunnett's multiple comparisons test. Values of $p < 0.05$ were considered statistically significant. All analyses were performed using GraphPad Prism 6.0 software (GraphPad Prism Software, Inc., San Diego, CA, USA).

3. Results and Discussion

3.1. Bioguided fractionation of $CHCl_3$ fraction and chemotaxonomic significance

The cytotoxic potential of ethanol extract and fractions obtained after CCV was investigated using the MTT test. After 72 hours of treatment, $CHCl_3$ fraction showed high cytotoxic activity against A2058 cells, exhibiting IC_{50} = 15.05 µg/ml. For this reason, we have chosen this fraction for the isolation of bioactive metabolites. Classical chromatographic procedures (column chromatography followed by TLC) resulted in the isolation of compounds **3, 4** and **5**. A mixture of two probable triterpenes (**1/2**) was also obtained directly from EE.

Table 1. Cytotoxic activity (IC_{50}, µg/ml)[a] of isolated compounds (**1–5**), ethanol extract (EE) and fractions ($CHCl_3$, AcOEt and MeOH) obtained from stem-barks of *C. quercifolius*. Vemurafenib (vemu) was used as standard drug.

Extract/fraction	**EE**	**$CHCl_3$**	**AcOEt**	**MeOH**	**-**
IC_{50} (µg/ml)*	15.52 ± 1.01	15.05 ± 1.04	28.51 ± 1.05	> 200	-
Compound	**1/2**	**3**	**4**	**5**	**Vemu**

IC_{50} (µg/ml)	> 200 µM	> 200 µM	40.90 µM	161.90 µM	5.63 µM

[a]Concentration required for 50% cell growth inhibition. [*]Results are expressed as mean ± S.E.M.

All isolated compounds were unambiguously identified by NMR (1D and 2D) analysis, as well as comparison with data reported in the literature. Compounds **1** and **2** were identified as an inseparable mixture of the lupeol-3β-*O*-cinnamate and lupeol-3β-*O*-dihydrocinnamate triterpenes [11]. Compound **3** was identified as lupeol-3β-*O*-hexanoate [31]. Compounds **4** and **5** were identified as the bis-*nor*-diterpenes phyllacanthone [11] and favelanone [14], respectively. Chemical structures of the compounds are shown in Figure 2. NMR data are shown in supplementary material.

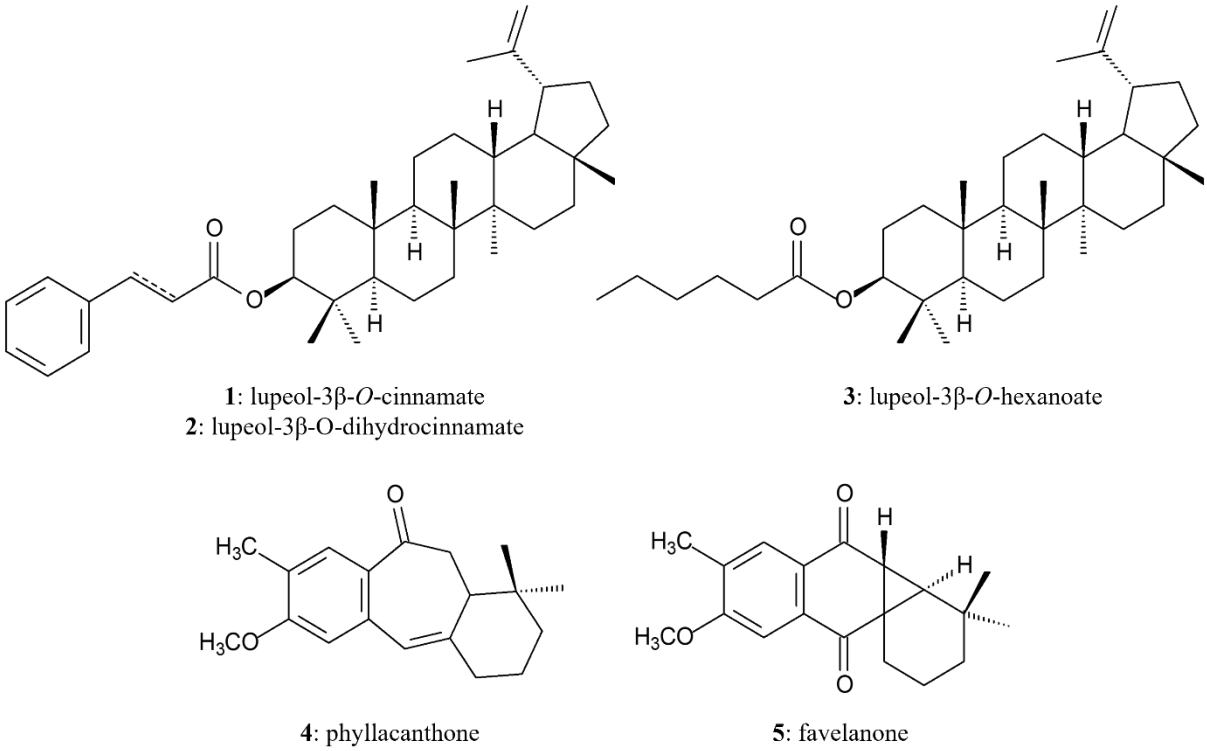

Figure 2. Chemical structures of compounds isolated from $CHCl_3$ fraction.

Many lupane-type triterpenes have been reported in the *Cnidoscolus* genus. Lupeol was purified from *C. quercifolius* [17], *C. multilobus* (Pax) Johnst (and *C. texanus* (Muell.-Arg.) Small (syn.: *Jatropha texanus* Muell.-Arg.) extracts. Lupeol-3β-*O*-acetate was also reported in *C. texanus* and *C. multilobus* [32]. Lupeol-3β-*O*-nanoate was isolated from *C. quercifolius* [17] and *C. vitifolius* [31]. In this investigation, we describe the isolation and characterization of three lupane-type triterpenes: lupeol-3β-*O*-cinnamoyl (**1**), lupeol-3β-*O*-dihydrocinnamoyl (**2**) and lupeol-3β-*O*-hexanoate (**3**) from the stembarks of *C. quercifolius*. Compounds **1** and **2** are commonly reported in this species [11,17]. In contrast, this study is the first to report the presence of **3** in *C. quercifolius*. We also described the isolation of two bis-*nor*-diterpenes (**4** and **5**). Phyllacanthone (**4**) was commonly and exclusively found in *C. quercifolius* [11,14,15,17], suggesting that this compound is a chemical marker of this plant.

3.2. Cytotoxic activity of phyllacanthone (PHY)

After obtention, all isolated compounds were tested against melanoma cells (1 – 200 µM). As shown in table 1, compound **4** (phyllacanthone, PHY) demonstrated moderate cytotoxic potential, presenting IC_{50} = 40.9 µM. Remaining molecules were inactive (**1/2** and **3**, IC_{50} > 200 µM) or weakly active (**5**, IC_{50} = 161.9 µM). PHY inhibited cell growth in a concentration-dependent manner, resulting in cell mortality increased by 82% upon treatment with 100 µM (Figure 3). As A2058 is considered a drug resistant cell line [19,21,33], we performed complementary assays to better understand the antimelanoma potential of PHY.

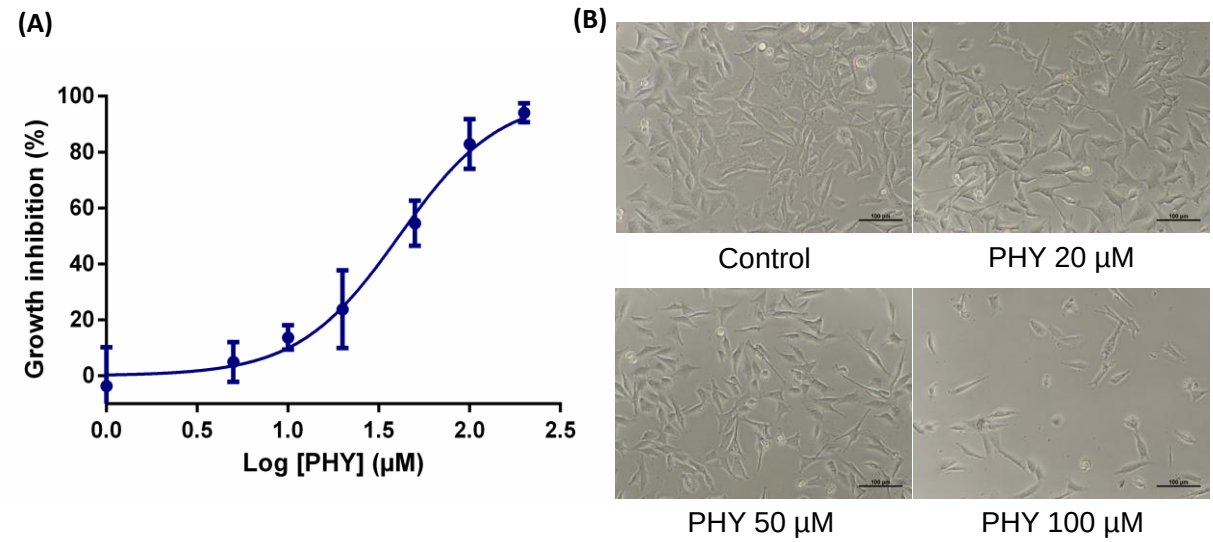

Figure 3. Effect of PHY on A2058 cells viability. Cells were grown in the presence of increasing concentrations of PHY (1 – 200 µM) for 72h and then cell viability was determined by MTT assay. Growth inhibition values are expressed as mean ± SEM (A). Photomicrographs (B) show reduction of cell density after 72h of exposure to increasing concentrations of PHY (20, 50 and 100 µM), compared to untreated cells (control).

3.4. PHY induces apoptosis in A2058 cells

Given that apoptosis is one of the most common mechanisms evoked by natural cytotoxic molecules, the pro-apoptotic effect of PHY was determined by double fluorescence staining with annexin-V and 6-CFDA. As shown in figure 4, PHY (50 and 100 µM) increased the number of annexin-V and 6-CFDA double-stained cells compared to untreated cells (control), indicating a significant pro-apoptotic effect. Treated cells also showed typical apoptotic features, including rounding cell, cell shrinkage and blebbing, especially after PHY 100 µM treatment. No morphological changes were evidenced in control cells.

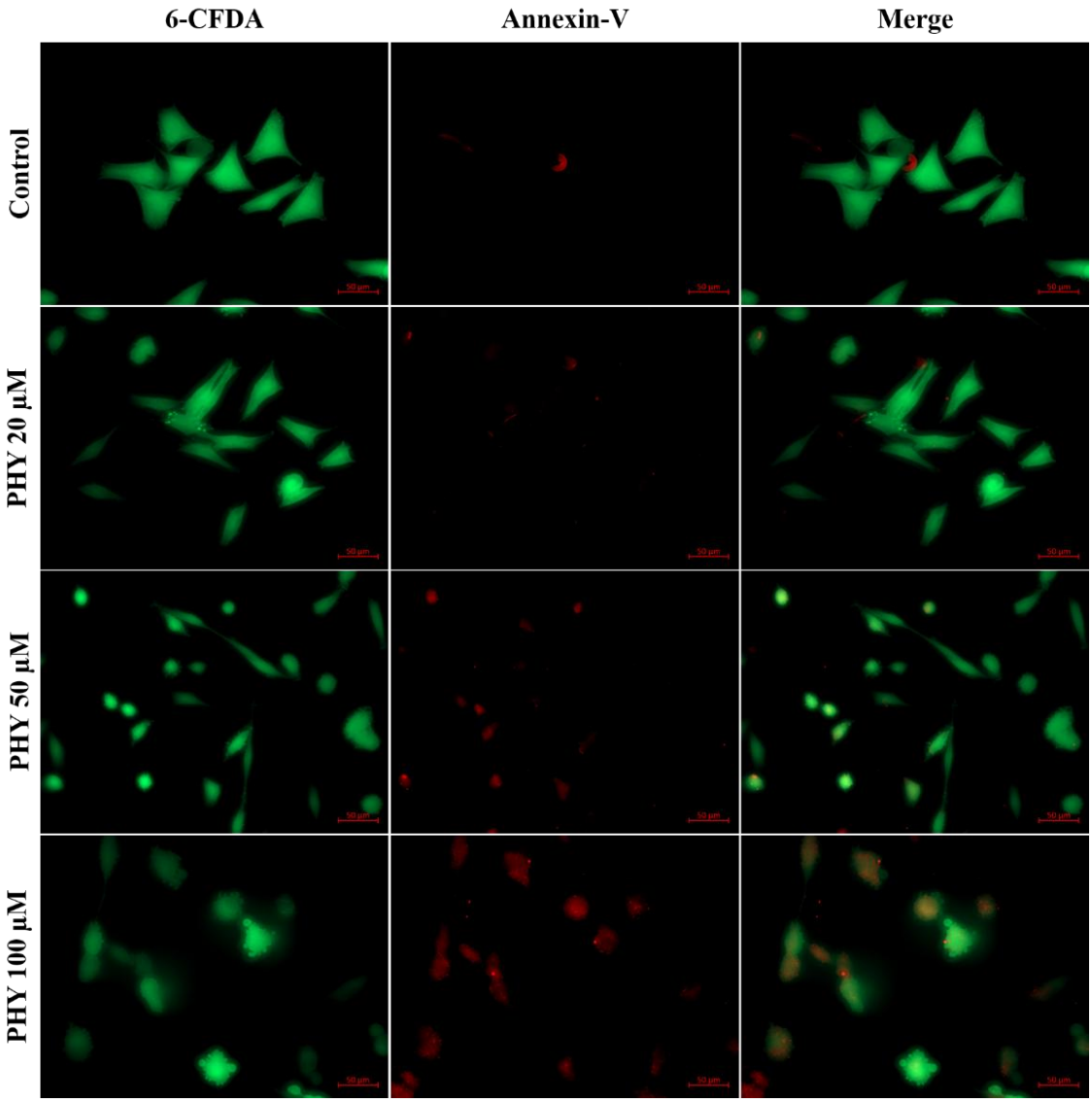

Figure 4. Pro-apoptotic effect of PHY (20, 50 and 100 µM) on A2058 melanoma cells. Photomicrographs were obtained after 72h of treatment using annexin-V/6-CFDA double staining.

Caspase-3 activity was measured to confirm the pro-apoptotic activity of PHY. Caspase activation is one of the most important hallmarks of apoptosis. This family of proteases recognize and cleave target proteins only after an aspartic acid residue. Caspase-3 is an effector caspase and displays essential role in both intrinsic and extrinsic apoptosis pathways. It cleaves multiple cellular substrates, including DNA, cell membrane components,

and cytoskeleton proteins, resulting in cell dismantling and apoptosis [34]. After 72h of treatment, PHY (20, 50 and 100 µM) increased caspase-3 activity compared to untreated cells (p<0.05), confirming its capacity to induce apoptosis in melanoma cells (Figure 5).

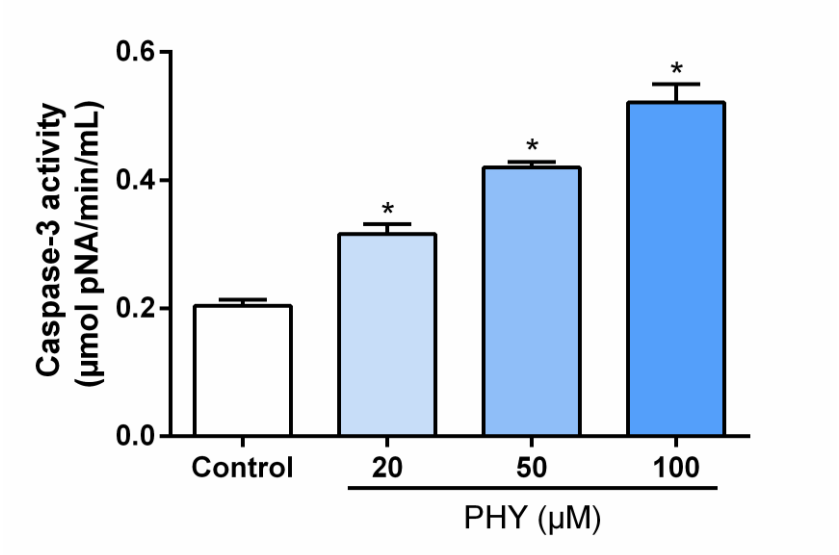

Figure 5. Caspase-3 activation induced by PHY (20, 50 and 100 µM). Data are expressed as mean ± SEM, *p<0.05 (vs. control group), according to ANOVA one-way followed by Dunnett's post-test (n = 3).

3.5. PHY induces cell cycle arrest

To assess whether the cytotoxic effect of PHY was associated with changes in cell cycle progression, A2058 cells were treated with different concentrations of the diterpene (20, 50 and 100 µM) and analyzed by flow cytometry. Cell cycle phases distribution was determined according to DNA content, stained with propidium iodide solution, as previously reported [33]. After 72h of treatment, PHY promoted a significant G0/G1 and S cell arrest at the expense of G2/M cell population (p<0.05), confirming the previously observed pro-apoptotic effect (Figure 6).

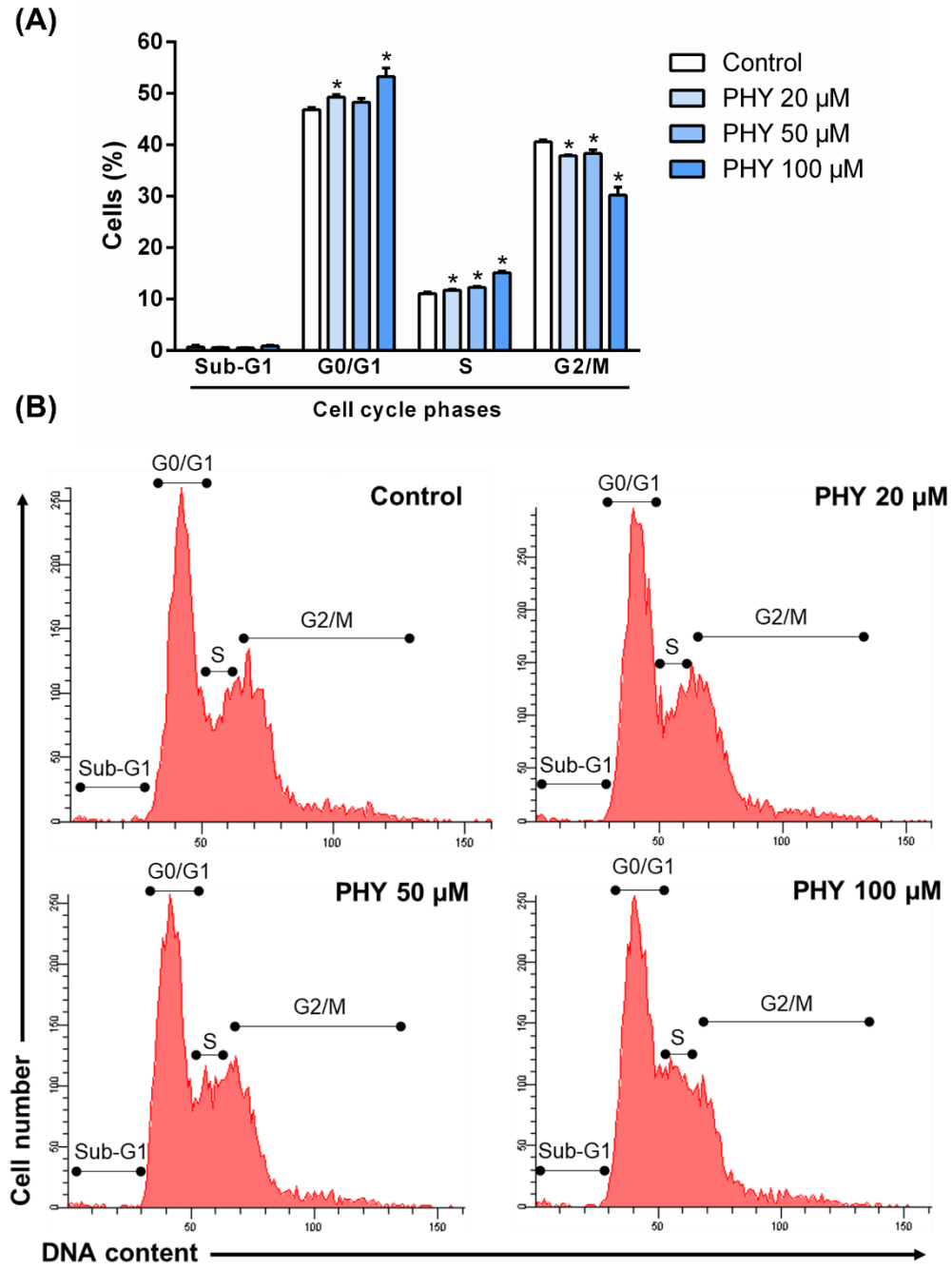

Figure 6. Effects of PHY (20, 50 and 100 µM) on different phases of the cell cycle (Sub-G1, G0/G1, S, G2/M). After 72h of treatment, cells were stained with propidium iodide solution and measured by flow cytometry as shown in the quantitative cell phases distribution (A) and in the representative histograms (B). Data are expressed as mean ± SEM (n = 3), *p<0.05 (*vs.* control group, untreated cells) according to one-way ANOVA followed by Dunnett's post-test.

3.6. PHY inhibits cell migration

As melanoma cells have high invasive and metastatic potential, it is suitable to evaluate the effect of new antimelanoma agents on cell migration. In this study, A2058 cells were treated with PHY (20 and 50 µM) and cell motility was assessed by wound healing assay. As presented in Figure 6, PHY (50 µM) reduced cell migration into the zone free of cells during all the experiment (3 – 24h), compared to untreated cells ($p<0.05$). Cell migration inhibition is often associated with alterations in key proteins of the cell cytoskeleton, such as actin filaments and microtubules [35,36]. These proteins ensure not only increased cell resistance but are also capable of inducing cell remodeling during cell migration, which is essential for tumor development. Considering that PHY was able to induce cell cycle arrest at G0/G1 and inhibit cell migration, we evaluated its influence on the polymerization of tubulin, a microtubule-forming protein.

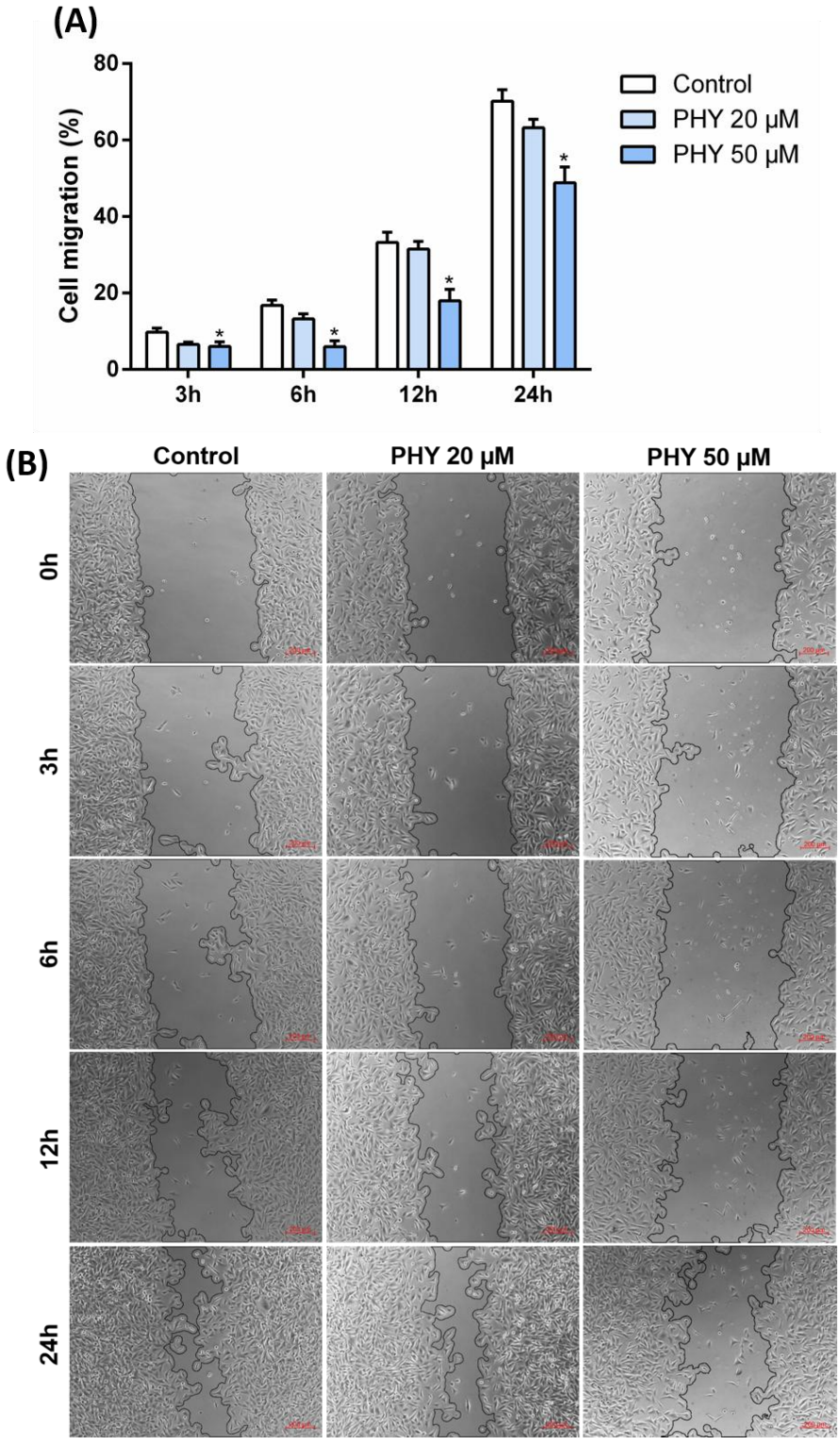

Figure 7. Effet oh PHY (20 and 50 µM) on cell migration after 3, 6, 12 and 24h of treatment (A). Photomicrographs illustrate cell migration into the zone free of cells according to the treatment (B). Data are expressed as mean ± SEM, **p*<0.05 (*vs.* control, ANOVA one-way followed by Dunnett's post-test), from at least three independent measurements.

3.7. PHY induces tubulin depolymerization

To assess the effect of PHY on cytoskeleton integrity, melanoma cells were exposed to PHY (20, 50 and 100 μM) for 24h and then microtubules were stained with a FITC-conjugated anti-α-tubulin monoclonal antibody. DAPI was employed to stain DNA content and cells were visualized under fluorescence microscope. As expected, untreated cells (control) appeared as fusiform cells with ramifications, presenting typical structural network, with tubulin chains anchored near the cell-cell contact sites and organized along the apical-basis axis (Figure 8). In contrast, PHY-treated cells (especially with 50 and 100 μM) showed cell shrinkage and rounding morphology with accumulation of tubulin near the nucleus. The same cell alterations were observed after treatment with nocodazole (50 nM), a standard cytotoxic molecule capable of interacting with α-tubulin residues and destabilizing microtubule formation.

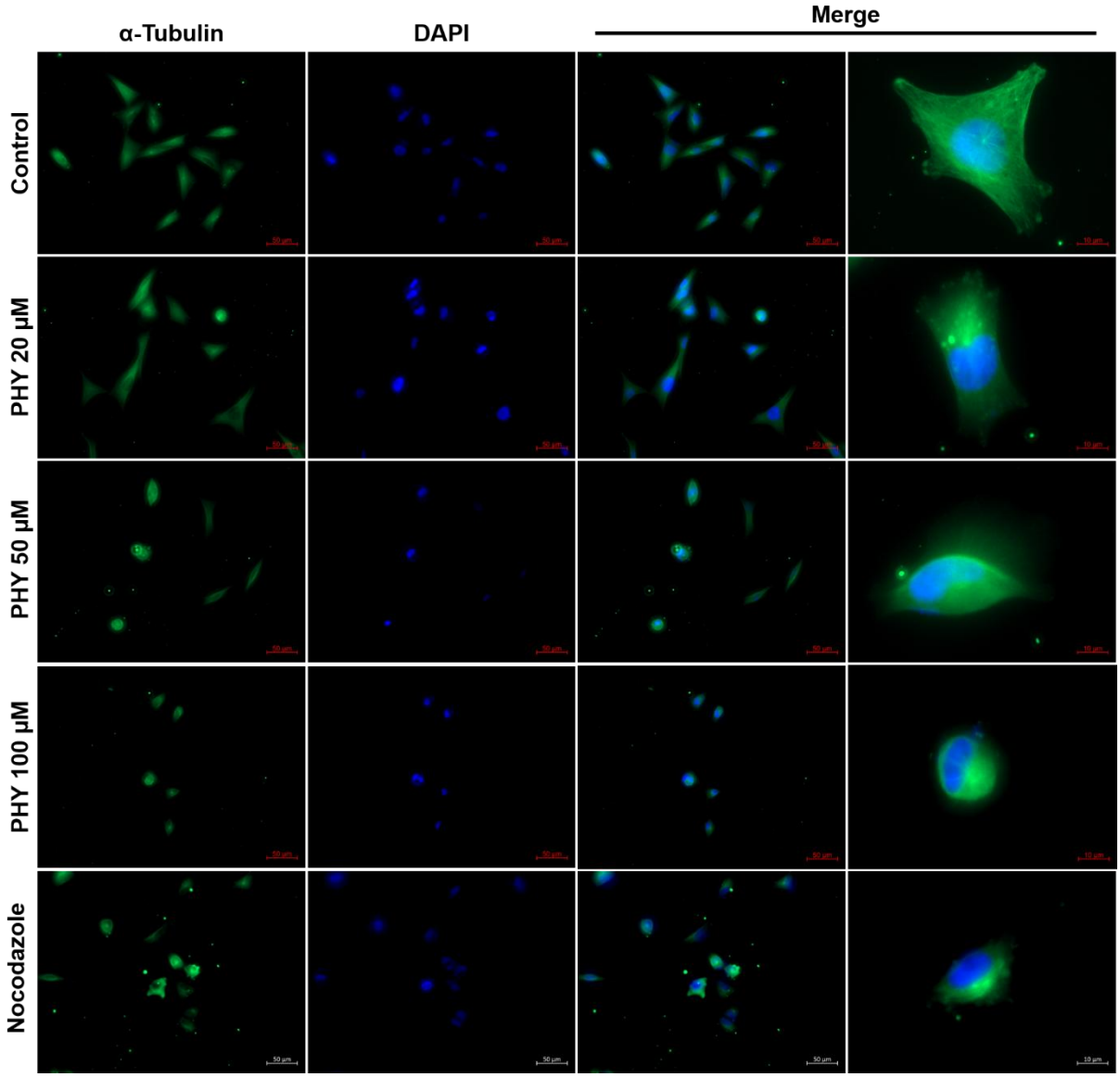

Figure 8. Effect of PHY (20, 50 and 100 µM) and nocodazole (50 nM) on α-tubulin polymerization after 24h of treatment. Cells were fixed, permeabilized and α-tubulin was stained with a FITC-conjugated anti-α-tubulin monoclonal antibody. Photomicrographs were taken under fluorescence microscope. Note intact microtubule network in untreated A2058 cells, while PHY(50 and 100 µM) and nocodazole-treated cells showed rounding morphology and perinuclear accumulation of tubulin.

Cytoskeleton disruption is a cellular event closely linked to apoptosis. Activation of effector caspases, such as caspase-3, triggers cleavage of several proteins which are important

for maintaining cell integrity, including cytoskeleton proteins, transmembrane and nuclear proteins. Consequently, cells exhibit reduced remodeling capacity, limited motility, cytoplasmic contraction, and nuclear fragmentation, resulting in the formation of apoptotic bodies [37]. Combined, pharmacological data show that the cytotoxic effect of PHY seems to be associated with a pro-apoptotic activity involving cytoskeleton dismantling via tubulin depolymerization, as observed for nocodazole. Concerning antimelanoma therapy, there is no clinically used drug that exerts anticancer activity via tubulin depolymerization to date. To confirm this hypothesis, we describe next a molecular docking study using tubulin and PHY chemical structures.

3.8. Docking study

Molecular docking procedures were performed to evaluate a possible interaction between PHY and tubulin. This protein can be modulated by nocodazole (NOC) (compound used as standard in experimental protocol) and colchicine (COL), compounds with great structural differences that interact in proximal but different binding sites, displaced between the A and B domains of tubulin [24]. This difference in binding site as well as in the structural profile of these two compounds corresponds to the binding with different amino acids.

Redocking procedures were performed with complexes between tubulin and the crystallographic ligands nocodazole and colchicine. Table 2 shows that both redocking procedures had success, with RMSD values for the best poses of NOC and COL lower than 2.0 Å, with energy values less than -8.0 Kcal/mol. Figure 9 illustrates the best redocked geometries, showing the excellent match and then validating the Vina algorithm for these systems.

Table 2. Binding energies (Kcal/mol) and RMSD values for all the docked compounds.

Entry	Compound	Binding Energy (Kcal/mol)	RMSD crystal (Å)	RMSD u.b. (Å)	RMSD l.b. (Å)
1	Colchicine (best)	-10.0	0.188	-	-
2	Nocodazole (best)	-9.0	1.085	-	-
3	PHY_{col} (conf. 1)	-8.3	-	0.000	0.000
4	PHY_{col} (conf. 2)	-8.0	-	2.292	6.553
5	PHY_{col} (conf. 3)	-8.0	-	2.069	6.475
6	PHY_{col} (conf. 4)	-7.8	-	2.233	3.478
7	PHY_{col} (conf. 5)	-7.4	-	2.247	4.071
8	PHY_{col} (conf. 6)	-7.3	-	1.368	1.825
9	PHY_{col} (conf. 7)	-6.9	-	2.385	4.455
10	PHY_{col} (conf. 8)	-6.7	-	2.144	6.263
11	PHY_{col} (conf. 9)	-6.6	-	2.075	3.055
12	PHY_{noc} (conf. 1)	-4.2	-	0.000	0.000
13	PHY_{noc} (conf. 2)	-3.2	-	3.113	6.119
14	PHY_{noc} (conf. 3)	-1.8	-	2.386	6.009
15	PHY_{noc} (conf. 4)	-1.6	-	1.757	2.489
16	PHY_{noc} (conf. 4)	-1.3	-	1.710	6.778

*"col" indicates the docking using the tubulin originally complexed with colchicine. "noc" indicates the use of nocodazole complex. "RMSD crystal" is related to the crystallographic conformations; "RMSD u.b." matches each atom in one conformation with itself in the other conformation, ignoring any symmetry; "RMSD l.b." matches each atom in one conformation with the closest atom of the same element type in the other conformation, being calculated as the maximum value between atoms c1,c2 and c2,c1.

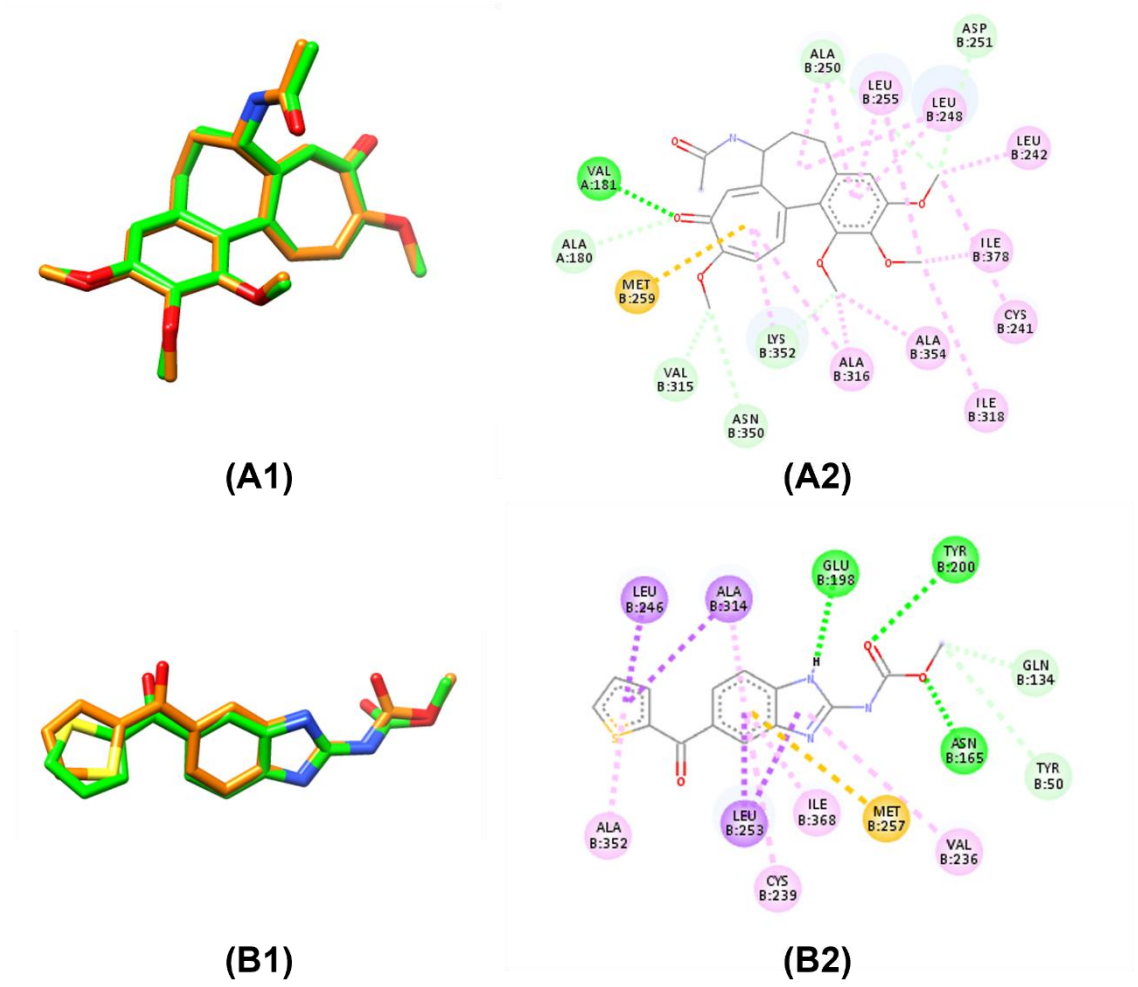

Figure 9. 3D images and 2D diagrams for the best poses of redocking results (structures in green) for colchicine (A1 and A2) and nocodazole (B1 and B2), comparing with the correspondent crystallographic ligands (in orange). *Colors in 2D diagrams: in green, conventional hydrogen bonds; in light blue, carbon hydrogen bond; in purple, pi-sigma bond; in dark yellow, pi-sulfur bond; in pink, alkyl or pi-alkyl bond.*

Considering the results of PHY dockings, Table 2 shows that the best energy conformations were founded considering the specific binding site of colchicine, where the energy value of the best pose was -8.3 Kcal/mol. On the other hand, poor interactions were made by PHY considering the binding site of nocodazole (-4.2 for the best pose). The number

of poses generated by Vina algorithm was different because this software ranks the conformations and shows only the most representative (nine using COL binding site and five using NOC binding site) of each subset of near conformers. In general, we can attribute these results to the structural profile of this diterpene, which is closer to the colchicine considering the three fused rings, the atom types and then their physical-chemical profile and possibilities of interactions. Figure 10 shows in details the interactions of PHY docked in the colchicine binding site from tubulin. As presented in the figure, the partially symmetrical distribution of the atoms and rings in PHY structure can explain the flip in some conformations with near energy values (the poses with a distance 0.5 Kcal/mol from the best pose are presented in the Figure 10).

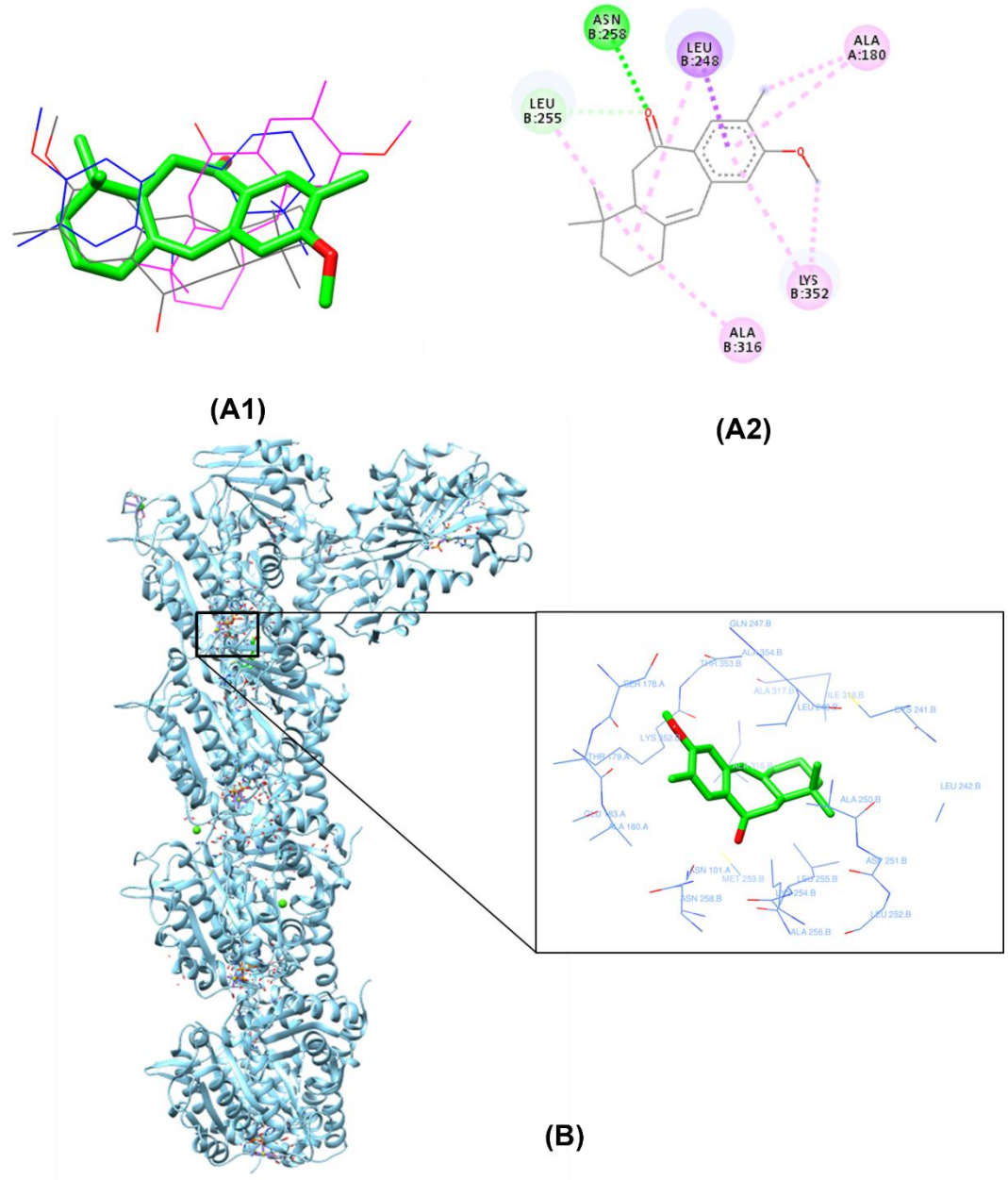

Figure 10. (A1) the four best poses for PHY in the colchicine binding site of tubulin (*green sticks – best 1; gray wireframe – best 2; blue wireframe – best 3; magenta wireframe – best 4*). (A2) The best pose (-8.3 Kcal/mol) in 2D diagram (*Colors in 2D diagrams: in green, conventional hydrogen bonds; in light blue, carbon hydrogen bond; in purple, pi-sigma bond; in pink, alkyl or pi-alkyl bond).* (B) 3D representation of tubulin (blue chains) and colchicine binding site containing PHY (compound in green).

4. Conclusion

A bioguided purification approach led to the isolation of phyllacanthone (PHY), a cytotoxic bis-*nor*-diterpene commonly found in *C. quercifolius* stembarks. This compound inhibited cell proliferation and migration, and induced apoptosis and cell arrest in both G0/G1 and S phases. Immunofluorescence assays suggested these findings were related to cytoskeleton disruption promoted by a tubulin depolymerization effect. Molecular docking data confirmed this hypothesis and revealed satisfactory interaction between PHY and tubulin, particularly at the colchicine binding site. From this study, it will be possible to design new PHY-structure based molecules to obtain antimelanoma drug candidates.

Acknowledgments

This work was accomplished through technical-scientific collaboration by Franco-Brazilian Network on Natural Products (FB2NP). The authors also thank to FACEPE (*Fundação de Amparo à Ciência e Tecnologia do Estado de Pernambuco*) for the master's scholarship granted (RGOJ).

References

[1] R.M. MacKie, A. Hauschild, A.M.M. Eggermont, Epidemiology of invasive cutaneous melanoma, Ann. Oncol. 20 (2009) vi1–vi7. https://doi.org/10.1093/annonc/mdp252.

[2] E.H. Tracey, A. Vij, Updates in Melanoma, Dermatol. Clin. 37 (2019) 73–82. https://doi.org/10.1016/j.det.2018.08.003.

[3] A. Platz, S. Egyhazi, U. Ringborg, J. Hansson, Human cutaneous melanoma: a review of NRAS and BRAF mutation frequencies in relation to histogenetic subclass and body site, Mol. Oncol. 1 (2008) 395–405. https://doi.org/10.1016/j.molonc.2007.12.003.

[4] V. Umansky, A. Sevko, Melanoma-induced immunosuppression and its neutralization,

Semin. Cancer Biol. 22 (2012) 319–326. https://doi.org/10.1016/j.semcancer.2012.02.003.

[5] I. Lugowska, P. Teterycz, P. Rutkowski, Immunotherapy of melanoma, Contemp. Oncol. 22 (2018) 61–67. https://doi.org/10.5114/wo.2018.73889.

[6] A. Niezgoda, P. Niezgoda, R. Czajkowski, Novel approaches to treatment of advanced melanoma: A review on targeted therapy and immunotherapy, Biomed Res. Int. 2015 (2015) 851387. https://doi.org/10.1155/2015/851387.

[7] R. Dummer, D. Schadendorf, P.A. Ascierto, A. Arance, C. Dutriaux, A.M. Di Giacomo, P. Rutkowski, M. Del Vecchio, R. Gutzmer, M. Mandala, L. Thomas, L. Demidov, C. Garbe, D. Hogg, G. Liszkay, P. Queirolo, E. Wasserman, J. Ford, M. Weill, L.A. Sirulnik, V. Jehl, V. Bozón, G. V. Long, K. Flaherty, Binimetinib versus dacarbazine in patients with advanced NRAS-mutant melanoma (NEMO): a multicentre, open-label, randomised, phase 3 trial, Lancet Oncol. 18 (2017) 435–445. https://doi.org/10.1016/S1470-2045(17)30180-8.

[8] P.B. Chapman, A. Hauschild, C. Robert, J.B. Haanen, P. Ascierto, J. Larkin, R. Dummer, C. Garbe, A. Testori, M. Maio, D. Hogg, P. Lorigan, C. Lebbe, T. Jouary, D. Schadendorf, A. Ribas, S.J. O'Day, J.A. Sosman, J.M. Kirkwood, A.M.M. Eggermont, B. Dreno, K. Nolop, J. Li, B. Nelson, J. Hou, R.J. Lee, K.T. Flaherty, G.A. McArthur, Improved survival with vemurafenib in melanoma with BRAF V600E mutation, N. Engl. J. Med. 364 (2011) 2507–2516. https://doi.org/10.1056/NEJMoa1103782.

[9] C. Robert, B. Karaszewska, J. Schachter, P. Rutkowski, A. Mackiewicz, D. Stroiakovski, M. Lichinitser, R. Dummer, F. Grange, L. Mortier, V. Chiarion-Sileni, K. Drucis, I. Krajsova, A. Hauschild, P. Lorigan, P. Wolter, G. V. Long, K. Flaherty, P. Nathan, A. Ribas, A.M. Martin, P. Sun, W. Crist, J. Legos, S.D. Rubin, S.M. Little, D. Schadendorf, Improved overall survival in melanoma with combined dabrafenib and trametinib, N. Engl. J. Med. 372 (2015) 30–39. https://doi.org/10.1056/NEJMoa1412690.

[10] U.P. de Albuquerque, P.M. de Medeiros, A.L.S. de Almeida, J.M. Monteiro, E.M. de

Freitas Lins Neto, J.G. de Melo, J.P. dos Santos, Medicinal plants of the caatinga (semi-arid) vegetation of NE Brazil: A quantitative approach, J. Ethnopharmacol. 114 (2007) 325–354. https://doi.org/10.1016/j.jep.2007.08.017.

[11] T.L.G. de Lemos, E.R. Silveira, M.F. Oliveira, R. Braz Filho, C.D. Hufford, Terpenoids from *Cnidoscolus phyllacanthus* Pax et Hoff , J. Braz. Chem. Soc. 2 (1991) 105–110. https://doi.org/10.5935/0103-5053.19910023.

[12] Y. Endo, T. Ohta, S. Nozoe, Neofavelanone, A novel tetracyclic cyclobutene derivative from the Brazilian plant, *Cnidoscolus phyllacanthus*, Tetrahedron Lett. 33 (1992) 353–356. https://doi.org/10.1016/S0040-4039(00)74129-3.

[13] T. Ohta, Y. Endo, R. Kikuchi, C. Kabuto, N. Harada, S. Nozoe, Absolute stereochemistry of benzocycloheptenone derivatives from *Cnidoscolus phyllacanthus*, Tetrahedron. 50 (1994) 5659–5668. https://doi.org/10.1016/S0040-4020(01)85636-2.

[14] Y. Endo, T. Ohta, S. Nozoe, Favelines, novel tricyclic benzocycloheptenes with cytotoxic activities from brazilian plant, *Cnidoscolus phyllacanthus*, Tetrahedron Lett. 32 (1991) 3083–3086. https://doi.org/10.1016/0040-4039(91)80695-3.

[15] R.G. de Oliveira-Júnior, C.A. Alves Ferraz, M.C. Pontes, N.B. Cavalcante, E.C. da Cruz Araújo, A.P. de Oliveira, L. Picot, L.A. Rolim, J.R.G. da Silva Almeida, Antibacterial activity of terpenoids isolated from *Cnidoscolus quercifolius* Pohl (Euphorbiaceae), a Brazilian medicinal plant from Caatinga biome, Eur. J. Integr. Med. 24 (2018) 30–34. https://doi.org/10.1016/j.eujim.2018.10.011.

[16] J.T. da S.P. Sobrinho, E.A. Tavares, V.T.N. de A. Castro, J. Veras-Filho, G.C.G. Militão, T.G. Silva, E.L.C. Amorim, Antiproliferative activity of species of the genus *Cnidoscolus* against HT-29, Hep-2 and NCI-H292 cells, Mol. Clin. Pharmacol. 3 (2012) 55–61. https://www.researchgate.net/publication/260191306.

[17] A.C. Paula, K.M. Melo, A.M. Da Silva, D.A. Ferreira, F.J.Q. Monte, G.M.P. Santiago,

T.L.G. Lemos, R. Braz-Filho, G.C.G. Militão, P.B.N. Da Silva, T.G. Da Silva, Chemical constituents and cytotoxic activity of *Cnidoscolus phyllacanthus*, Rev. Virtual Quim. 8 (2016) 231–241. https://doi.org/10.5935/1984-6835.20160015.

[18] R. Ronca, E. Di Salle, A. Giacomini, D. Leali, P. Alessi, D. Coltrini, C. Ravelli, S. Matarazzo, D. Ribatti, W. Vermi, M. Presta, Long Pentraxin-3 Inhibits Epithelial-Mesenchymal Transition in Melanoma Cells, Mol. Cancer Ther. 12 (2013) 2760–2771. https://doi.org/10.1158/1535-7163.MCT-13-0487.

[19] R.G. de Oliveira Júnior, A. Bonnet, E. Braconnier, H. Groult, G. Prunier, L. Beaugeard, R. Grougnet, J.R.G. da Silva Almeida, C.A.A. Ferraz, L. Picot, Bixin, an apocarotenoid isolated from *Bixa orellana* L., sensitizes human melanoma cells to dacarbazine-induced apoptosis through ROS-mediated cytotoxicity, Food Chem. Toxicol. 125 (2019) 549–561. https://doi.org/10.1016/j.fct.2019.02.013.

[20] T. Mosmann, Rapid colorimetric assay for cellular growth and survival: Application to proliferation and cytotoxicity assays, J. Immunol. Methods. 65 (1983) 55–63. https://doi.org/10.1016/0022-1759(83)90303-4.

[21] C. Juin, R.G. de Oliveira Junior, A. Fleury, C. Oudinet, L. Pytowski, J.B. Bérard, E. Nicolau, V. Thiéry, I. Lanneluc, L. Beaugeard, G. Prunier, J.R.G.D.S. Almeida, L. Picot, Zeaxanthin from Porphyridium purpureum induces apoptosis in human melanoma cells expressing the oncogenic BRAF V600E mutation and sensitizes them to the BRAF inhibitor vemurafenib, Brazilian J. Pharmacogn. 28 (2018) 457–467. https://doi.org/10.1016/j.bjp.2018.05.009.

[22] C. Juin, R.G. de Oliveira Junior, A. Fleury, C. Oudinet, L. Pytowski, J.-B. Bérard, E. Nicolau, V. Thiéry, I. Lanneluc, L. Beaugeard, G. Prunier, J.R.G.D.S. Almeida, L. Picot, Zeaxanthin from *Porphyridium purpureum* induces apoptosis in human melanoma cells expressing the oncogenic BRAF V600E mutation and sensitizes them to the BRAF inhibitor

vemurafenib, Rev. Bras. Farmacogn. 28 (2018) 457–467. https://doi.org/10.1016/j.bjp.2018.05.009.

[23] J. Cisilotto, L.P. Sandjo, L.G. Faqueti, H. Fernandes, D. Joppi, M.W. Biavatti, T.B. Creczynski-Pasa, Cytotoxicity mechanisms in melanoma cells and UPLC-QTOF/MS2chemical characterization of two Brazilian stingless bee propolis: Uncommon presence of piperidinic alkaloids, J. Pharm. Biomed. Anal. 149 (2018) 502–511. https://doi.org/10.1016/j.jpba.2017.11.038.

[24] Y. Wang, H. Zhang, B. Gigant, Y. Yu, Y. Wu, X. Chen, Q. Lai, Z. Yang, Q. Chen, J. Yang, Structures of a diverse set of colchicine binding site inhibitors in complex with tubulin provide a rationale for drug discovery, FEBS J. 283 (2016) 102–111. https://doi.org/10.1111/febs.13555.

[25] H.M. Berman, J. Westbrook, Z. Feng, G. Gilliland, T.N. Bhat, H. Weissig, I.N. Shindyalov, P.E. Bourne, The protein data bank, Nucl. Acids Res. 28 (2000) 235–242.

[26] O. Trott, A. Olson, Autodock vina: improving the speed and accuracy of docking with a new scoring function, efficient optimization and multithreading, J. Comput. Chem. 31 (2010) 455–461. https://doi.org/10.1002/jcc.21334.AutoDock.

[27] G.M. Morris, R. Huey, W. Lindstrom, M.F. Sanner, R.K. Belew, D.S. Goodsell, A.J. Olson, AutoDock4 and AutoDockTools4: Automated docking with selective receptor flexibility, J. Comput. Chem. 30 (2009) 2785–2791. https://doi.org/10.1002/jcc.21256.

[28] M.J. Frisch, G.W. Trucks, H.B. Schlegel, G.E. Scuseria, M.A. Robb, J.R. Cheeseman, G. Scalmani, V. Barone, G.A. Petersson, H. Nakatsuji, X. Li, M. Caricato, A. Marenich, J. Bloino, B.G. Janesko, R. Gomperts, M. Mennucci, H.P. Hratchian, J. V Ortiz, A.F. Izmaylov, J.L. Sonnenberg, D. Williams-Young, F. Ding, F. Lipparini, F. Egidi, J. Goings, B. Peng, A. Petrone, T. Henderson, D. Ranasinghe, V.G. Zakrzewski, J. Gao, N. Rega, G. Zheng, W. Liang, M. Hada, M. Ehara, K. Toyota, R. Fukuda, J. Hasegawa, M. Ishida, T. Nakajima, Y.

Honda, O. Kitao, H. Nakai, T. Vreven, K. Throssell, J.A. Montgomery, J.E. Peralta, F. Ogliaro, M. Bearpark, J.J. Heyd, E. Brothers, K.N. Kudin, V.N. Staroverov, T. Keith, R. Kobayashi, J. Normand, K. Raghavachari, A. Rendell, J.C. Burant, S.S. Iyengar, J. Tomasi, M. Cossi, J.M. Millam, M. Klene, C. Adamo, R. Cammi, J.W. Ochterski, R.L. Martin, K. Morokuma, O. Farkas, J.B. Foresman, D.J. Fox, Gaussian 09, Revision A.02, (2016).

[29] E.F. Pettersen, T.D. Goddard, C.C. Huang, G.S. Couch, D.M. Greenblatt, E.C. Meng, T.E. Ferrin, UCSF Chimera - a visualization system for exploratory research and analysis, J. Comput. Chem. 25 (2004) 1605–1612.

[30] S. Maestro, Schrödinger Release 2019-2, (2019).

[31] R.L. Brum, N.K. Honda, S.C. Hess, A.J. Cavalheiro, F. Delle Monache, Acyl lupeols from *Cnidoscolus vitifolius*, Phytochemistry. 49 (1998) 1127–1128. https://doi.org/10.1016/S0031-9422(98)00069-7.

[32] G. Delgado, J. Hernandez, M.Y. Rios, M.I. Aguilar, Pentacyclic triterpenes from *Cnidoscolus multilobus*, Planta Med. 60 (1994) 390. https://doi.org/10.1055/s-2006-959515.

[33] R.G. de Oliveira-Júnior, N. Marcoult-Fréville, G. Prunier, L. Beaugeard, E. Beserra de Alencar Filho, E.D. Simões Mourão, S. Michel, L.J. Quintans-Júnior, J.R. Guedes da Silva Almeida, R. Grougnet, L. Picot, Polymethoxyflavones from *Gardenia oudiepe* (Rubiaceae) induce cytoskeleton disruption-mediated apoptosis and sensitize BRAF-mutated melanoma cells to chemotherapy, Chem. Biol. Interact. 325 (2020) 109109. https://doi.org/10.1016/j.cbi.2020.109109.

[34] A.G. Porter, R.U. Ja, Emerging roles of caspase-3 in apoptosis, Cell Death Differ. 6 (1999) 99–104.

[35] A. Ganguly, H. Yang, R. Sharma, K.D. Patel, F. Cabral, The role of microtubules and their dynamics in cell migration, J. Biol. Chem. 287 (2012) 43359–43369. https://doi.org/10.1074/jbc.M112.423905.

[36] S. Povea-Cabello, M. Oropesa-Ávila, P. de la Cruz-Ojeda, M. Villanueva-Paz, M. De La Mata, J.M. Suárez-Rivero, M. Álvarez-Córdoba, I. Villalón-García, D. Cotán, P. Ybot-González, J.A. Sánchez-Alcázar, Dynamic reorganization of the cytoskeleton during apoptosis: The two coffins hypothesis, Int. J. Mol. Sci. 18 (2017) 1–14. https://doi.org/10.3390/ijms18112393.

[37] O. Ndozangue-Touriguine, J. Hamelin, J. Bréard, Cytoskeleton and apoptosis, Biochem. Pharmacol. 76 (2008) 11–18. https://doi.org/10.1016/j.bcp.2008.03.016.